and

$$b_I(\theta)=\frac{1}{\sqrt{2}k}\sum_{l=1}^{\infty}\frac{1}{2i}(e^{2i\delta_{lI}^{+}}-e^{2i\delta_{lI}^{-}})P_l^1(\cos\theta)\,, \quad \text{(A3)}$$

where $\delta_{I\delta}^{+}$ is the phase shift for the wave with isotopic spin I, orbital angular momentum l, and total angular momentum $(l+\frac{1}{2})$; δ_{lI}^{-} is the corresponding phase shift for total angular momentum $(l-\frac{1}{2})$; $P_l(\cos\theta)$ and $P_{l1}(\cos\theta)$ are the Legendre polynomials and associated Legendre functions of the indicated order, respectively; and k is the c.m. system momentum of the incident K^+ in units of $\hbar$.

PHYSICAL REVIEW VOLUME 173, NUMBER 5 25 SEPTEMBER 1968

Elastic Scattering and Single-Pion Production in Proton-Proton Interactions at 6.92 BeV/c

G. ALEXANDER, Z. CARMEL,* Y. EISENBERG, E. E. RONAT, A. SHAPIRA, AND G. YEKUTIELI
Department of Nuclear Physics, The Weizmann Institute of Science, Rehovoth, Israel

AND

A. FRIDMAN,† G. MAURER, J. OUDET, C. ZECH,‡ AND P. CÜER
Département de Physique Corpusculaire, Centre de Recherches Nucléaires de Strasbourg, Strasbourg, France

(Received 29 April 1968)

Elastic scattering and single-pion production in pp collisions at 6.92 BeV/c were studied in the BNL 80-in. hydrogen bubble chamber. Partial cross sections for the different final states are given. The reaction $pp\to nN_{1238}^{*}(p\pi^{+})$ with $\sigma=1.9\pm0.3$ mb is analyzed and is in agreement with the modified one-pion-exchange model. Single-pion production can be explained as due mainly to two channels: (a) $pp\to N_{1238}^{*}(p\pi^{+})n$, and (b) $pp\to p(n\pi^{+})$ or $pp\to p(p\pi^{0})$, where the $(n\pi^{+})$ and $(p\pi^{0})$ pairs are in an $I=\frac{1}{2}$ state.

I. INTRODUCTION

THE results on two-prong events reported here are part of a more general study on pp interactions at 6.92 BeV/c. We have investigated in this paper the elastic and inelastic pp reactions associated with two-prong events. The production of strange particles in pp collisions at 6.92 BeV/c is studied in another paper.[1] The present analysis of the two-prong events and in particular the evaluation of the cross sections for the various competing channels and isobars, follows closely the method used in a similar study of pp collisions at 5.5 BeV/c.[2]

The general experimental procedure and the identification of events are described in Sec. II. Results on elastic scattering are given in Sec. III. In Sec. IV single-pion production and isobar production are studied. The production and decay of the N_{1238}^{*} isobar is compared with one-pion exchange models in Sec. V, and in Sec. VI the mechanism of pion production is analyzed.

II. EXPERIMENTAL

The experiment is based on 64 000 pictures taken at the 80-in. hydrogen bubble chamber (HBC) exposed to the AGS proton beam in Brookhaven National Laboratory. Measurements on a sample of long beam tracks yielded an incident momentum of 6.92 ± 0.075 BeV/c. The contamination in the beam was estimated by the δ-rays method, and a total contamination of K^+, π^+, μ^+, and e^+ less than 1.2% was found.[3] A total pp collision cross section of 42.6 ± 1.3 mb was found. The total cross-section value is based on some 20 000 pp events scanned with 98% efficiency; it also includes 1.9 ± 0.3 mb correction for loss of small-angle elastic scatterings.

The analysis of the two-prong events is based on a sample of 5980 measured events. The total cross section for two-prong events is 28.4 ± 0.3 mb and each event in this experiment corresponds to 4.9 μb. The data were analyzed by the THRESH and GRIND programs, and verified by ionization estimation. In the first stage of analysis the two-prong events were fitted to the following three final states (see Table I): (a) pp elastic scattering, (b) $pn\pi^{+}$, and (c) $pp\pi^{0}$. The missing-mass-square histograms of these hypotheses are shown on Fig. 1. In this way 3107 events fitted uniquely a single final-state hypothesis, 167 events fitted two or more hypotheses, and the remaining events did not fit any of the reactions (a), (b), or (c).

* Also submitted as part of a Ph.D. thesis at the Weizmann Institute of Science, 1968.

† Also from Institut für Hochenergiephysik, Universität Heidelberg, Heidelberg, Germany.

‡ Present address: Institut für Hochenergiephysik, Universität Heidelberg, Heidelberg, Germany.

[1] G. Alexander, A. Shapira, E. Simopoulou, and G. Yekutieli, Nuovo Cimento **53**, 455 (1968).

[2] G. Alexander, O. Benary, G. Czapek, B. Haber, N. Kidron, B. Reuter, A. Shapira, E. Simopoulou, and G. Yekutieli, Phys. Rev. **154**, 1284 (1967).

[3] R. Atar, M.Sc. thesis, Weizmann Institute of Science, 1967 (unpublished).

TABLE I. Cross sections of the identified final states of two-prong events.

Final state	Cross section (mb)	Final state	Cross section (mb)
(a) pp	11.4±0.5[a]	(d) ppMM[b]	2.1±0.2
(b) $pn\pi^+$	5.2±0.4	(e) $p\pi^+$MM[c]	6.6±0.5
(c) $pp\pi^0$	2.0+0.2	(f) $\pi^+\pi^+$MM	1.2±0.2

[a] Including 1.9±0.3 mb correction for small angles.
[b] Not including events belonging to (a) and (c).
[c] Not including events belonging to (b).

The events with no fit are due to reactions with two or more neutral particles in the final state. A selected sample of these events was further analyzed with the missing-mass (MM) hypotheses: (d) ppMM, (e) $p\pi^+$MM, and (f) $\pi^+\pi^+$MM (see Table I). This analysis and the results on two and more pion production in two-prong events will be reported in another paper.

Few events (24) fitted reaction (a) as well as reaction (b) or (c). With further analysis all these events were accepted as elastic scattering cases. There were 143 cases of ambiguity between the final states (b) $pn\pi^+$ and (c) $pp\pi^0$; 56 of them were due to ambiguity between the two final states $p\pi^+n$ and π^+pn. All these ambiguities are mainly due to a forward energetic particle of near-minimum ionization that could be either a proton or a pion.

A similar kind of ambiguity can also occur between the final states: (b) $pn\pi^+$ and (d) ppMM. All the ambiguities were decided upon by a peripheral test. The study of events uniquely identified as (b) $pn\pi^+$, (c) $pp\pi^0$, (d) ppMM, and (e) $p\pi^+$MM shows that in the c.m. system the baryons are emitted in opposite directions and in a very small cone around the pp line of interaction. The ambiguities are then resolved by rejection of the hypothesis associated with the smaller quantity

$$|\cos\theta^*(B_1)-\cos\theta^*(B_2)|$$

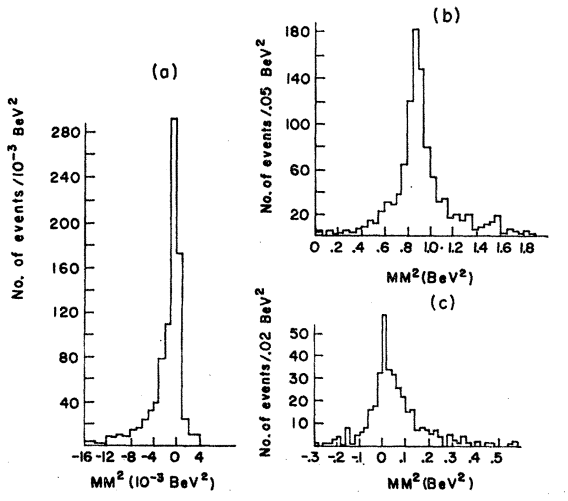

FIG. 1. Missing-mass-squared distributions of the final states: (a) pp, (b) $pn\pi^+$, and (c) $pp\pi^0$ in pp collisions.

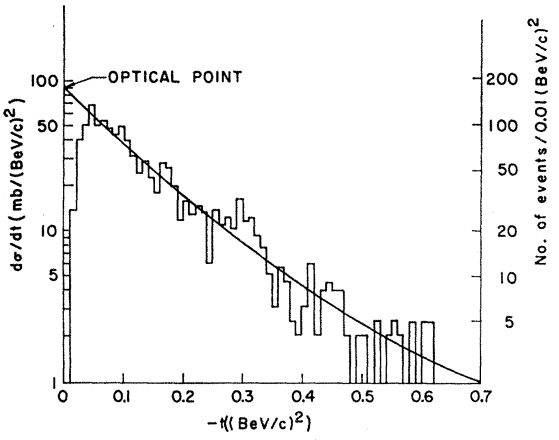

FIG. 2. Differential cross section of the reaction $pp \rightarrow pp$. The solid line represents the best fit of the data to the expression $d\sigma/dt = e^{A+Bt+Ct^2}$.

[the $\theta^*(B)$'s are the c.m. production angles of the baryons].

The application of the peripheral test and the rejection of the nonperipheral events improve the sample indeed, the corrected angular distributions become symmetric, as expected in the final state of pp collisions.

The cross sections for the various final states of the two-prong events are summarized in Table I.

III. ELASTIC SCATTERING

The differential cross section $d\sigma/dt$, folded around 90°, of 1780 pp elastic scattering events is plotted in Fig. 2. It appears from this plot that there is a loss of events with small momentum transfer. The azimuthal scattering angle ψ around the incident proton was plotted for different intervals of momentum transfer. Asymmetry in the azimuthal distribution, connected with the loss of dipping scattered protons, was found only for low momentum transfer. Following earlier work in similar range of momentum,[2] the observed differential cross section in the interval $0.04 \leq |t| \leq 0.5$ $(\text{BeV}/c)^2$ was fitted to the expression $d\sigma/dt = e^{A+Bt+Ct^2}$. The best values obtained are $e^A = 94.0 \pm 2.5$ mb $(\text{BeV}/c)^{-2}$, $B = 9.03 \pm 0.15$ $(\text{BeV}/c)^{-2}$, and $C = 3.68 \pm 0.6$ $(\text{BeV}/c)^{-4}$. The area under the fitted differential-cross-section curve, corresponds to a total elastic cross section of 11.4±0.5 mb, of which 9.5±0.4 mb are due to the observed events, and 1.9±0.3 mb is a correction for the missing small-angle scatterings. With this small-angle correction the total pp collision cross section at 6.92 BeV/c is 42.6±1.3 mb. The fitted differential cross section extrapolated to $t=0$ gives a value $d\sigma/dt(t=0) = 94.0 \pm 2.5$ mb/$(\text{BeV}/c)^2$ in the forward direction. This value, although within statistical error of the optical point $[\sigma_{\text{tot}}^2/16\pi = 92.6 \pm 5.0$ mb/$(\text{BeV}/c)^2]$, is somewhat higher than the latter and may indicate some small contribution from the real part, Re$f(0)$, of

TABLE II. Total and elastic cross sections in pp collisions.

P_{inc} (BeV/c)	σ_{total} (mb)	$\sigma_{elastic}$ (mb)
4.03[a]	42.14±0.4	
4.55[a]	41.45±0.4	
4.97[a]	41.17±0.4	
5.52[a]	40.88±0.4	
5.52[b]	41.6 ±1.4	11.9±0.3
6.8[c]		11.8±0.2
6.92[d]	42.6 ±1.3	11.4±0.5
7.8[a]	40.08±0.05	
10.0[e]	40.0 ±0.3	
10.8[e]		11.0±0.2

[a] See Ref. 4.
[b] See Ref. 2.
[c] K. J. Foley, S. J. Lindenbaum, W. A. Love, S. Ozaki, J. J. Russell, and L. C. L. Yuan, Phys. Rev. Letters **11**, 425 (1963).
[d] This experiment.
[e] G. Belletini, G. Cocconi, A. N. Diddens, E. Lille, J. Pahl, J. P. Scanlon, J. Walters, A. M. Wetherell, and P. Zanella, Phys. Letters **14**, 164 (1965).

the elastic scattering amplitude in the forward direction:

$$|\alpha| = |\mathrm{Re}f(0)/\mathrm{Im}f(0)| = 0.12\pm0.20.$$

This value is very sensitive to the total cross section σ_{tot} and is in agreement with the value $\alpha=-0.3$ found by others[4] in this range of momentum.

The observed differential cross section in the smaller interval $0.04\leq|t|\leq0.12$ (BeV/c)^2 was also fitted to the expression $d\sigma/dt=e^{A+bt}$. The best values obtained are $e^A=89.3\pm6.7$ mb/(BeV/c)^2 and $b=7.7\pm0.5$ (BeV/c)$^{-2}$. This fit gives somewhat lower value for $d\sigma/dt(t=0)$ than the three-parameter fit. At the same time it yields the same total elastic cross section: $\sigma_{el}=e^A/b=11.5\pm0.5$ mb.

The pp differential cross section $d\sigma/dt=e^{A+bt}$ for small momentum transfer is like that of absorbing sphere with radius $r=2\sqrt{b}=1.10\pm0.04$ F.

The results of the present experiment are summarized and compared in Table II with similar ones in the same momentum range. It appears from Table II that, in general, present results on pp scattering agree with earlier ones.

IV. SINGLE-PION PRODUCTION

The two final states $pn\pi^+$ and $pp\pi^0$ are the only channels in pp collisions that lead to single-pion production.

The c.m. system angular distribution (Fig. 3) and momentum-transfer distributions (Fig. 4) of the nucleons show that the reactions $pp\rightarrow pn\pi^+$ and $pp\rightarrow pp\pi^0$ are highly peripheral.

The momentum-transfer square $\Delta^2(N_1)$ of a nucleon in the peripheral reaction $p_1p_2\rightarrow N_1N_2\pi$ was defined as $\Delta^2(N_1)=$ minimum of $\Delta^2(N_1\rightarrow p_1)$, $\Delta^2(N_1\rightarrow p_2)$, where $\Delta^2(N_1\rightarrow p_1)$ and $\Delta^2(N_1\rightarrow p_2)$ are the two possible Δ^2 values with respect to the two initial protons. For highly peripheral events it is possible, in this way,

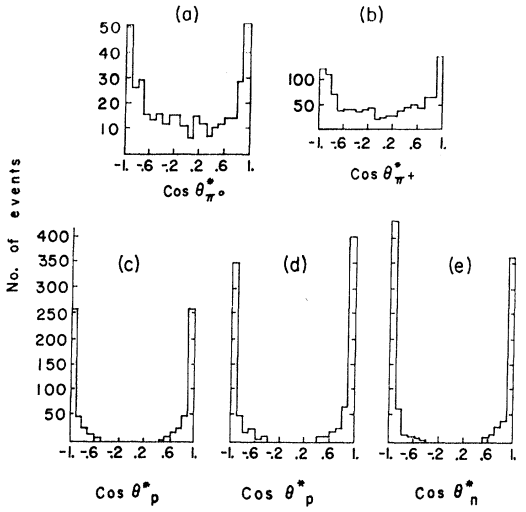

FIG. 3. Angular distributions (in the c.m. system) of pions and nucleons in the final states $pp\pi^0$ and $pn\pi^+$.

to associate each of the outgoing nucleons N_1N_2 with its appropriate incident proton. It is found that in the present sample, when $\Delta^2(N_1)=\Delta^2(N_1\rightarrow p_1)$, then always $\Delta^2(N_2)=\Delta^2(N_2\rightarrow p_2)$, and this seems to prove that the choice of the momentum transfer is suitable in this experiment. The differential-momentum-transfer distributions of the nucleons in the final states $pn\pi^+$ and $pp\pi^0$ can be represented by exponential functions: $d\sigma/dt=Ae^{Bt}$ for small $|t|$, where $t(N_1)=-\Delta^2(N_1)$. The fitted slopes are given in Table III. It appears from this table that in the interval $0.05<-t<0.4$ (BeV/c)^2

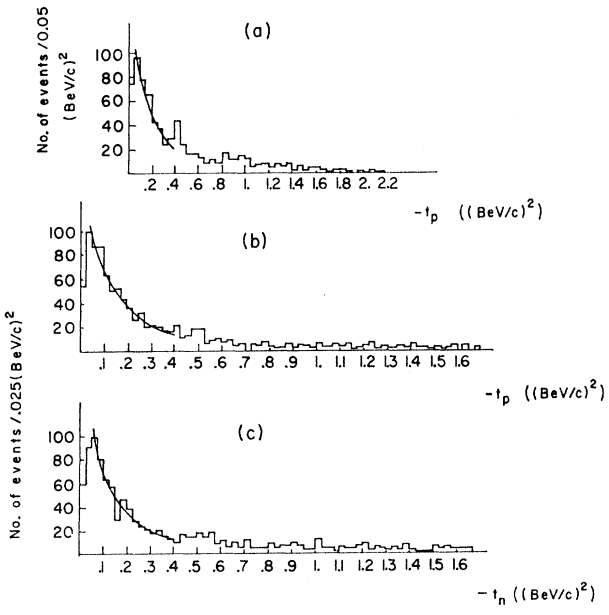

FIG. 4. Differential cross section distribution (dN/dt); number of events as function of momentum transfer to one of the outgoing nucleons (a) for the protons in $pp\pi^0$, (b) for the proton in $pn\pi^+$, and (c) for the neutron in $pn\pi^+$. The solid lines represent dN/dt as $\exp(6t)$.

[4] D. N. Bugg, S. C. Slater, G. H. Stafford, R. F. George, K. F. Riley, and R. J. Tapper, Phys. Rev. **146**, 980 (1966).

TABLE III. The slopes of various momentum-transfer distributions, of single nucleon: Ae^{Bt}; and of two nucleons: $ae^{b_1t_1+b_2t_2}$.

Final state	Particle	Single particle B (BeV/c)$^{-2}$	Two nucleons b_1 or/and b_2 (BeV/c)$^{-2}$
$pn\pi^+$	proton	5.7±0.3[a]	5.8±0.3[b]
$np\pi^+$	neutron	6.6±0.4[a]	6.1±0.3[b]
$pp\pi^0$	proton	5.0±0.5[a]	5.4±0.4[b]
$N_{1238}^*(p\pi^+)n$	N_{1238}^*	9.3±1.2	...

[a] For $0.04 < -t < 0.5$ (BeV/c)^2.
[b] For both $0.04 < -t_1 < 0.5$ and $0.04 < -t_2 < 0.5$ (BeV/c)^2.

practically all the nucleons have the same slope: $B \sim 6.0$ (BeV/c)$^{-2}$. In order to take account of the peripheral production of the nucleons an attempt was made to describe the invariant-mass distributions in the $pn\pi^+$ and $pp\pi^0$ final states by an ordinary phase space weighted by an e^{Bt} peripheral factor. However, as can be seen from Fig. 5, the Monte Carlo results for the invariant-mass distributions of $M(pp)$ and $M(pn)$ obtained in this way do not agree with the observed results. Better agreement is obtained with a double-momentum-transfer distribution

$$d^2\sigma/dt_1dt_2 = a\exp(b_1t_1+b_2t_2),$$

where $t_1 = -\Delta^2(N_1)$ and $t_2 = -\Delta^2(N_2)$. The fitted slopes of the two nucleons distribution function are given in Table III. Reasonable discriptions of various features are obtained when the ordinary phase space is multiplied by the peripheral factor $\exp[6(t_1+t_2)]$ (see Fig. 5).

The invariant-mass distributions of the $p\pi^+$, $n\pi^+$, and $p\pi^0$ combinations are given in Figs. 6, 7(a), and 7(b). The $p\pi^+$ invariant-mass distribution (Fig. 6) shows a pronounced N_{1238}^* peak. A fit with ordinary phase space for general background yielded 38% $N_{1238}^*(p\pi^+)$ isobar. The other invariant-mass distributions $M(n\pi^+)$ and $M(p\pi^0)$ do not show any clear isobar structure [see Figs. 7(a) and 7(b)]. Fits of an ordinary phase space, together with some isobars identified in pp collisions N_{1238}^*, N_{1400}^*, N_{1520}^*, and N_{1688}^*, did not yield satisfactory results. Better results are obtained when the ordinary phase space is multiplied by a peripheral factor, $\exp[6(t_1+t_2)]$, and reflection effects are properly accounted for.

The reflection effect of the $N_{1238}^*(p\pi^+)$ isobar on the $M(n\pi^+)$ invariant mass in the final state $pn\pi^+$,

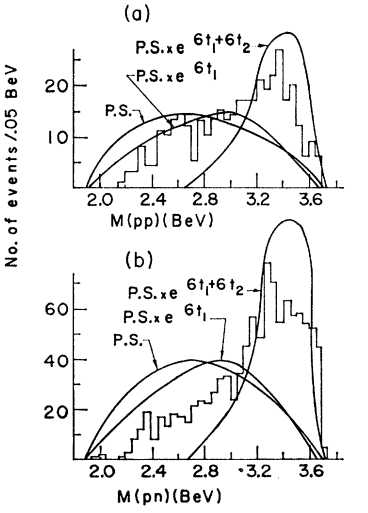

FIG. 5. Invariant-mass distributions of the two nucleons in the final states: (a) $pp\pi^0$ and (b) $pn\pi^+$.

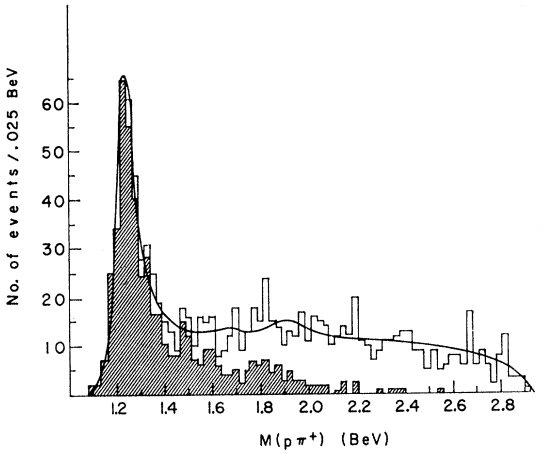

FIG. 6. Invariant-mass distribution of the $p\pi^+$ combination in the $pn\pi^+$ final state. The solid line represents a maximum-likelihood fit to phase space (56%), N_{1240}^{++} (38%), N_{1670}^{++} (2%), N_{1920}^{++} (4%), and N_{2360}^{++} (0%). The shaded area indicates events selected by MIM.

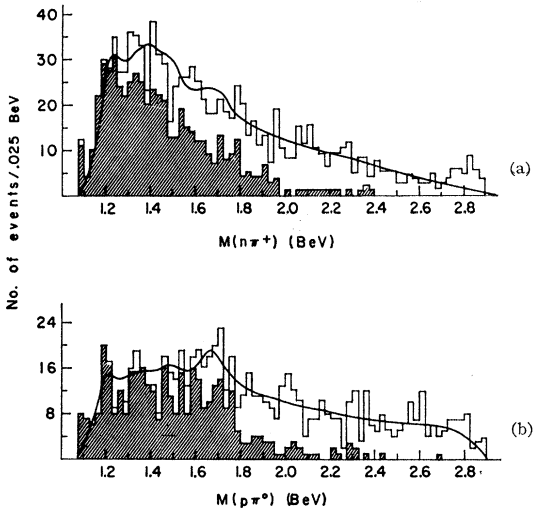

FIG. 7. (a) Invariant-mass distribution of the $n\pi^+$ combination in the $pn\pi^+$ final state. The solid line represents a maximum-likelihood fit to peripheral background (21%), $N_{1238}^*(p\pi^+)$ reflection (30%), $N_{1238}^*(n\pi^+)$ (9%), N_{1400}^*(29%), N_{1520}^* (5%), and N_{1688}^* (6%). The shaded area indicates events selected by MIM. (b) Invariant-mass distribution for the $p\pi^0$ combination in $pp\pi^0$. Each event is plotted twice corresponding to the two possible combinations: $p_1\pi^0$ or $p_2\pi^0$. The solid line represents the best fit to peripheral background (25%), $p\pi^0$ reflection (45%), $N_{1238}^*(p\pi^0)$ (7%), N_{1400} (5%), N_{1520}^* (7%), and N_{1688}^* (10%). The shaded area indicates events selected by MIM.

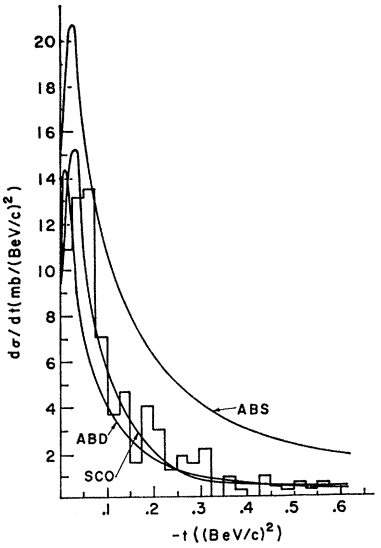

FIG. 8. Differential cross section $d\sigma/dt$ of the reaction $pp \to nN_{1238}^*(p\pi^+)$. The calculated curves are according to the three OPE models: (a) ABS, (b) ABD, and (c) SCO.

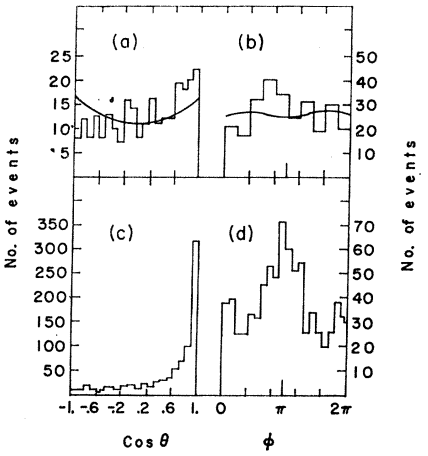

FIG. 9. Angular distributions of the decay proton in the rest system of the $p\pi^+$ pair: (a) and (b) when $1.1<M(p\pi^+)<1.35$ BeV; (c) and (d) outside this range.

was calculated by RANDSTAR[5] with a peripheral distribution $\exp(9t_{N^*})$. In the final state $p_1p_2\pi^0$ each event contributes twice to the invariant-mass distribution $M(p\pi^0)$. The contribution of the $p_2\pi$ combination to $M(p_1\pi^0)$ was simulated by the reflection of an ordinary phase space with a peripheral weighting factor $\exp(6t_{p_2})$. For consistency we have also to consider the reflection effect of the $n\pi^+$ combination on the $M(p\pi^+)$ effective mass. We tried to fit $M(p\pi^+)$ with the same reflection function as used for $M(p\pi^0)$. The results of this fit agree with those obtained for $M(p\pi^+)$ with an ordinary phase space. The best-fit curves for the $M(n\pi^+)$ and $M(p\pi^0)$ distributions are shown in Fig. 7. In these fits the phase space multiplied by the factor $\exp[6(t_1+t_2)]$ and the Breit-Wigner curves of the possible isobars N_{1400}^*, N_{1520}^*, and N_{1688}^* contribute to the same mass range. For this reason and because of the limited statistics of the present experiment, the best-fit analysis did not yield consistent production rates for the low-mass systems in the vicinity of the N_{1400}^*, N_{1520}^*, and N_{1688}^* isobars.

V. PRODUCTION AND DECAY OF THE N_{1238}^* ISOBAR

The analysis of the final-state $np\pi^+$ shows that in 38% of the events the following reaction takes place:

$$pp \to nN_{1238}^* \quad \text{and} \quad N^{*++} \to p\pi^+, \qquad (1)$$

corresponding to a production cross section of 1.9 ± 0.3 mb. The same analysis indicates that in the $1.15 \leq M(p\pi^+) \leq 1.33$ BeV mass range, most of the events belong to reaction (1) and the background is less than 15%. The sample of N_{1238}^* events was used to study the production and decay of the N^{*++} isobar in pp collisions at 6.92 BeV/c.

[5] G. Yekutieli, RANDSTAR, a Monte-Carlo computer program, Rehovot, 1965 (unpublished).

The differential cross section $d\sigma/dt$ of reaction (1) is shown in Fig. 8. Following Alexander *et al.*[6] and Haber and Yekutieli,[7] the experimental results are compared with three versions of the one-pion-exchange (OPE) model:

(1) Ordinary absorption model (ABS): The Born amplitude of the OPE diagram is modified by absorption effects in the incoming (pp) and outgoing (nN_{1238}^*) channels of reactions (1). The absorption effects are assumed to be the same for the pp and nN_{1238}^* interactions, and they are deduced from the analysis of pp elastic scattering data.

(2) Absorption model with different absorption effect for the nN_{1238}^* channel (ABD): Since there is no direct information on nN_{1238}^* interaction, the nN_{1238}^* absorption effect was treated as a free parameter and was found by best fit between theory and experiment.

(3) Sharp-cutoff model (SCO): In this model one assumes that only partial waves of the OPE amplitude with $J \geq J_c$ contribute to reaction (1). The SCO curve in Fig. 8 was calculated with $J_c=9$ which corresponds to an impact parameter $b=1$ F. This choice of J_c agrees with the observation of Haber and Yekutieli[7] that the SCO model with J_c corresponding to an impact parameter $b=1$ F explains well the differential cross section $d\sigma/dt$ of reaction (2) in the 3–15-BeV/c momentum range.

The angular distribution of the decay proton in the N_{1238}^* rest system can be written as[8]

$$W(\theta,\phi)\text{-}(3/4\pi)[\rho_{33}\sin^2\theta+(\tfrac{1}{2}-\rho_{33})(\tfrac{1}{3}+\cos^2\theta) - (2/\sqrt{3})(\mathrm{Re}\rho_{3,-1}\sin^2\theta\cos2\phi + \mathrm{Re}\rho_{3,1}\sin2\theta\cos\phi)]. \qquad (2)$$

[6] G. Alexander, B. Haber, A. Shapira, G. Yekutieli, and E. Gotsman, Phys. Rev. **144**, 1122 (1966).

[7] B. Haber and G. Yekutieli, Phys. Rev. **160**, 1410 (1967).

[8] K. Gottfried and J. D. Jackson, Nuovo Cimento **33**, 309 (1964).

TABLE IV. Density matrix elements ρ as functions of isobar production $\cos\theta^*$ values at 6.92 BeV/c.

$\lvert\cos\theta^*\rvert$	ρ_{33}	$\mathrm{Re}\rho_{3,1}$	$\mathrm{Re}\rho_{3,-1}$	$\rho_{33}(0.5-\rho_{33})-(\mathrm{Re}\rho_{3,-1})^2-(\mathrm{Re}\rho_{31})^2$
0.99–1.0	0.15±0.06	0.03±0.05	0.13±0.06	0.035±0.020
0.92–0.99	0.09±0.06	−0.05±0.05	0.10±0.06	0.025±0.024
0.92–0.97	0.35±0.09	0.04±0.07	0.16±0.06	0.057±0.035

Here the $\rho_{mm'}$ are the density matrix elements of the $J=\frac{3}{2}$ N^* produced in (1). The parameters in (2) were found by best-fit analysis of the data and are given in Table IV. The angular distribution of the decay protons of events with $1.15\leq M(p\pi^+)\leq 1.33$ BeV are given in Figs. 9(a) and 9(b); the solid lines represent best fit of (2) to the data. Similar distributions for events outside the N_{1238}^* mass range are shown for comparison on Fig. 9(c) and 9(d). It appears from Fig. 9 that a small contamination of non-N_{1238}^* events in the $1.15\leq M(p\pi^+)\leq 1.33$ BeV sample distorts the expected angular distributions of the decay protons.

The density matrix elements obey the following condition:

$$\rho_{33}(0.5-\rho_{33})-(\mathrm{Re}\rho_{3,1})^2-(\mathrm{Re}\rho_{3,-1})^2\geq 0 \qquad (3)$$

implied by the positivity of the spin-density matrix.[9] Moreover, if reaction (1) is dominated by one-pion exchange, relation (3) becomes equality.[10] The observed values of relation (3) are given in Table IV and they are above zero. The errors in Table IV do not take into account the effect of non-N_{1238}^* events in the present sample. Maor[11] showed that the one-pion-exchange equality condition (3) is very sensitive to small admixture of non-N_{1238}^* background, or to contributions of competing exchange mechanisms. We believe that the deviations from the one-pion-exchange condition can be explained, mainly, by the effect of non-N_{1238}^* background in the present sample.

The density matrix elements were also calculated according to the above-mentioned versions of the OPE model and the results are compared with the observed values (see Fig. 10).

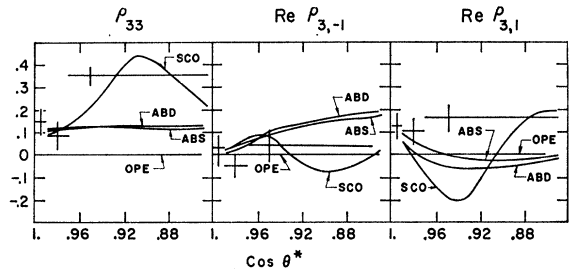

FIG. 10. The density matrix elements ρ_{33}, $\mathrm{Re}_{3,1}$, and $\mathrm{Re}\rho_{3,-1}$ as functions of the isobar production $\cos\theta^*$ values. The calculated values are according to the (1) OPE, (2) ABS, (3) ABD, and (4) SCO.

[9] P. Minnaert, Phys. Rev. **151**, 1306 (1966).

[10] G. A. Ringland and R. L. Thews, University of California Radiation Laboratory Report No. UCRL-18010, 1967 (unpublished).

[11] U. Maor (private communication).

VI. MECHANISM OF PION PRODUCTION

The analysis of the effective-mass distributions $M(p\pi^+)$, $M(n\pi^+)$, and $M(p\pi^0)$ shows strong $N_{1238}^*(p\pi^+)$ production, some $I=\frac{1}{2}$ low-mass systems in the vicinity of the N_{1400}^*, N_{1520}^*, and N_{1688}^* isobars and a peripheral background. Detailed analysis of the reaction $pp\rightarrow nN_{1238}^*(p\pi^+)$ in the momentum range 3–15 BeV/c[7] and also in the present experiment shows that it can be explained by a one-pion-exchange diagram with appropriate modifications. This reaction is also well explained by a Regge amplitude with a single-pion trajectory exchanged in the t channel.[12] An attempt is made to find out all other production mechanisms that contribute to the final states $pn\pi^+$ and $pp\pi^0$. Examination of the Dalitz plots of the $pn\pi^+$ and $pp\pi^0$ events (see Figs. 11 and 12) shows that the great majority of them are in the regions where $M^2(p\pi^+)$, $M^2(n\pi^+)$, and $M^2(p\pi^0)$ are small. Moreover, analysis of the $pn\pi^+$ and $pp\pi^0$ events shows that the concentration of events in regions with small $M(N\pi)$ on the Dalitz plots indicates that the two nucleons are emitted with small momentum transfers in opposite directions, while the pion is moving together with one of the nucleons. Following the above analysis and in an attempt to explain the production mechanism of single pions in the reaction $p_1p_2\rightarrow N_1N_2\pi$ it was assumed that (a) the pion is produced together with one nucleon (N_1), and (b) the pion together with

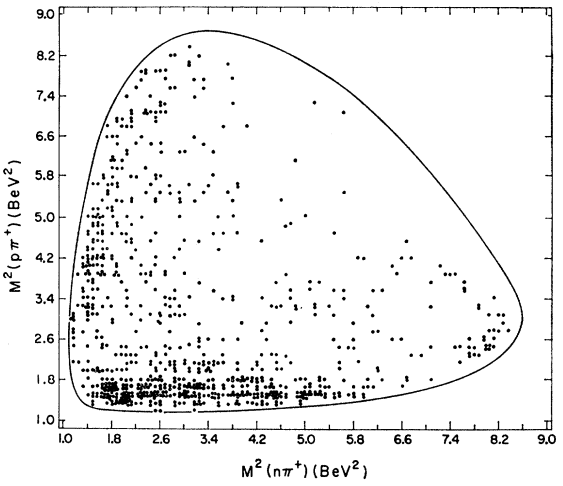

FIG. 11. Dalitz plot for the $pn\pi^+$ final state.

[12] B. Haber, U. Maor, G. Yekutieli, and E. Gotsman, Phys. Rev. **168**, 1773 (1968).

TABLE V. Cross sections of various final states in pp collisions as functions of the incident momentum.

P_{inc} (BeV/c)	Cross sections σ, in mb (1) $pn\pi^+$	(2) $pp\pi^0$	(3) nN_{1238}^{++}	(4) $(n\pi^+)_{\frac{1}{2}}$	(5) $(p\pi^0)_{\frac{1}{2}}$	σ_4/σ_5
2.8[a]	16.1±0.4	3.9±0.2	11.0 ±0.4	3.8±0.4	1.4±0.3	2.7±0.6
4.0[b]	9.7±0.4	2.6±0.3	4.8 ±0.4	4.3±0.3	1.5±0.3	2.8±0.6
5.52[c]	8.0±0.2	2.8±0.1	3.3 ±0.2	4.4±0.3	2.0±0.2	2.2±0.3
6.92[d]	5.2±0.4	2.0±0.2	1.9 ±0.3	3.0±0.5	1.5±0.3	2.0±0.5
10.0[e]	3.7±0.4		1.2 ±0.2	2.4±0.3		
28.5[f]	1.5±0.1		0.15±0.05	1.4±0.1		

[a] See Ref. 13.
[b] See Ref. 14.
[c] See Ref. 2.
[d] Present experiment.
[e] See Ref. 15.
[f] See Ref. 16.

that nucleon have minimum invariant mass (MIM), i.e.,

$$M(N_{1\pi})<M(N_{2\pi}).$$

With these assumptions the $np\pi^+$ events can be classified by the MIM criterion in two categories, corresponding to two exchange graphs:

(a) $M(p\pi^+)<M(n\pi^+)$: The π^+ and a proton are produced together in a $I=\frac{3}{2}$ state with an $I=1$ exchange.

(b) $M(n\pi^+)<M(p\pi^+)$: The π^+ and a neutron are produced together, with either an $I=1$ or an $I=0$ exchange.

The $p\pi^+$ and $n\pi^+$ combinations of the $pn\pi^+$ which were selected by MIM are shown by shaded areas on Figs. 6 and 7(a), respectively. It appears from Fig. 6 that almost all the $N_{1238}^*(p\pi^+)$ events were selected by MIM, and that the shaded $M(p\pi^+)$ mass distribution is made up of a single $N_{1238}^*(p\pi^+)$ isobar peak, with small nonresonance background. The invariant-mass distribution $M(n\pi^+)$, of $n\pi^+$ combinations selected by MIM [see shaded area of Fig. 7(a)], does not show any clear isobar structure. The MIM criterion was applied also to the $pp\pi^0$ events and in this way the ambiguity between the two protons in the final state $pp\pi^0$ could be resolved [see shaded area of Fig. 7(b)].

According to the MIM criterion the main contribution to the $I=\frac{3}{2}$ $p\pi^+$ state is due to N_{1238}^* production (not counting few events in the center of the Dalitz plot). This observation suggests that the exchange graph (a) (see Fig. 13) is due to the reaction $pp\rightarrow NN_{1238}^*$, and it can be described by one-pion-exchange amplitude A_π. The other exchange graph (b) (see Fig. 13) is very likely to be due to the diffraction scattering with an $I=0$ exchange and it can be described by the exchange of a Pomeranchuk trajectory with an amplitude A_p. Let us assume that single-pion production in pp collisions can be explained by the two amplitudes A_π and A_p.

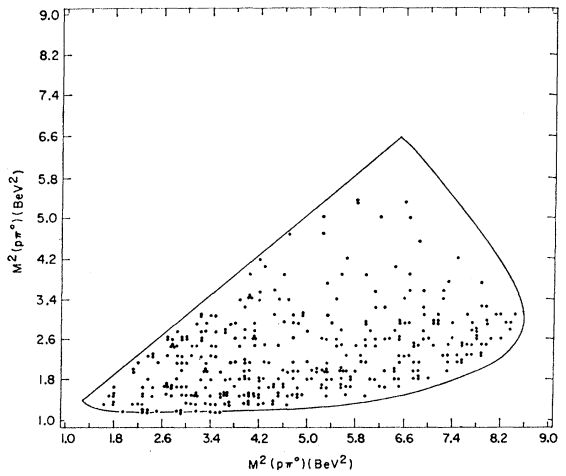

FIG. 12. Dalitz plot for the $pp\pi^0$ final state, folded around the symmetry axis.

At small momentum transfer there is no interference between A_π (real) and A_p (imaginary); therefore

$$\begin{aligned}\sigma(np\pi^+)&=(10/12)|A_\pi|^2+\tfrac{2}{3}|A_p|^2,\\ \sigma(pp\pi^0)&=(2/12)|A_\pi|^2+\tfrac{1}{3}|A_p|^2,\\ \sigma(nN_{1238}^*(p\pi^+))&=(9/12)|A_\pi|^2.\end{aligned}\tag{4}$$

In addition the cross sections for the $N\pi$ in the $I=\frac{1}{2}$ states are

$$\begin{aligned}\sigma(p(n\pi^+)_{1/2})&=\sigma(n\pi^+p)\\ &\quad-(10/9)\sigma(nN_{1238}^*(p\pi^+))=\tfrac{2}{3}|A_p|^2,\\ \sigma(p(p\pi^0)_{1/2})&=\sigma(pp\pi^0)\\ &\quad-(2/9)\sigma(nN_{1238}^*(p\pi^+))=\tfrac{1}{3}|A_p|^2.\end{aligned}\tag{5}$$

With this picture one expects that (1) at high energies $\sigma(nN_{1238}^*(p\pi^+))$ will decrease with incident momentum, while (2) $\sigma(p(n\pi^+)_{1/2})=2\sigma(p(p\pi^0)_{1/2})$ and will be constant at high energies.

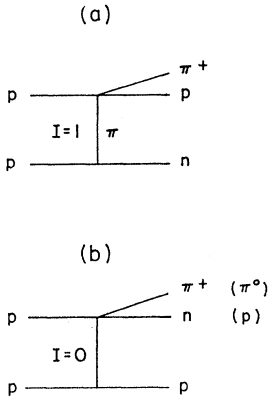

FIG. 13. Exchange diagrams of single-pion production in pp collisions.

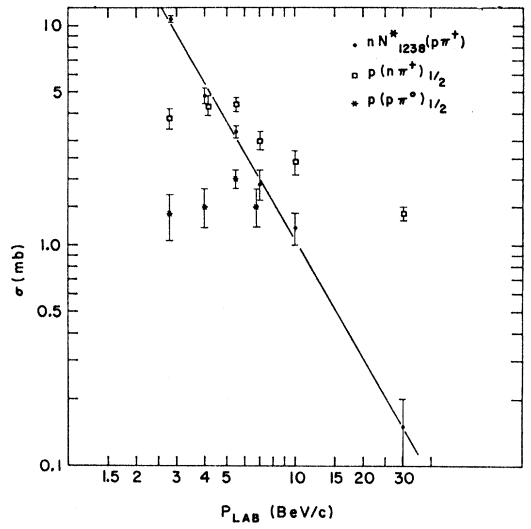

FIG. 14. Cross sections of the final state (a) $nN_{1238}^*(p\pi^+)$, (b) $p(n\pi^+)_{1/2}$, and (c) $p(p\pi^0)_{1/2}$ at incident momenta p-2.8 (Ref. 13), 4.0 (Ref. 14), 5.5 (Ref. 2), 6.5 (present experiment), 10.0 (Ref. 15), and 28.5 (Ref. 16) BeV/c.

These predictions can be compared with the results of several hydrogen-bubble-chamber experiments[2,13–16] on single-pion production in pp collisions.

Using the measured cross sections $\sigma(np\pi^+)$, $\sigma(pp\pi^0)$, and $\sigma(nN_{1238}^*)$, and assuming that (a) all $N\pi$ states with $I=\frac{3}{2}$ belong to N_{1238}^* and (b) there is no interference between $N\pi$ states with $I=\frac{3}{2}$ and $I=\frac{1}{2}$, the cross sections $\sigma(p(p\pi^+)_{1/2})$ and $\sigma(p(p\pi^0)_{1/2})$ of (4) were evaluated and are given in Table V and in Fig. 14.

The results show that (1) the $\sigma(p(p\pi^0)_{1/2})$ and $\sigma(p(n\pi^+)_{1/2})$ cross sections below 7.0 BeV/c do not decrease with energy, while at higher energies $\sigma(p(n\pi^+)_{1/2})$ decreases slowly with energy but less than $\sigma(nN_{1238}^*)$; (2) the ratio $\sigma(p(n\pi^+)_{1/2})/\sigma(p(p\pi^0)_{1/2})$ ≈ 2.0 as predicted if both $n\pi^+$ and $p\pi^0$ are in pure $I=\frac{1}{2}$ state. The agreement is good up to 7 BeV/c and it will be very desirable to have more measurements at higher incident momenta in order to have a better comparison between the model and the observation at higher energies.

Finally, one would like to know if the entire final state $p(N\pi)_{1/2}$ can be explained in terms of $N_{1/2}$ isobars produced in the reaction $pp \rightarrow pN_{1/2}$, with a subsequent decay $N_{1/2} \rightarrow N\pi$. Three $N_{1/2}$ isobars (N_{1400}^*, N_{1520}^*, and N_{1688}^*) were identified in pp production experiments[17,18] in the momentum range 4.0–30.0 BeV/c. Taking into account their relative decay width $\Gamma(N_{1/2} \rightarrow N\pi)$, these three isobars may contribute altogether less than 20% of the $p(N\pi)_{1/2}$ cross section below 7 BeV/c, while near 28 BeV/c the contributions of the $I=\frac{1}{2}$ isobars is less than 40%. It appears that with our present knowledge and also from this experiment, the major part of the $p(N\pi)_{1/2}$ final state seems to be nonisobaric peripheral background.

ACKNOWLEDGMENTS

We would like to thank Brookhaven National Laboratory, and the crews of the AGS and the 80-in. hydrogen bubble chamber for enabling us to obtain this exposure. Our thanks are also due to Professor H. Harari and Dr. U. Maor for fruitful comments. We are also grateful to Dr. B. Haber for his kind help.

[13] W. J. Fickinger, E. Pickup, D. K. Robinson, and E. Salant, Phys. Rev. **125**, 2082 (1962); T. C. Bacon, F. M. Bomse, T. B. Cochran, W. J. Fickinger, E. R. Goza, E. W. K. Hopkins, and E. O. Salant, *ibid.* **162**, 1320 (1967).

[14] S. Colleti, J. Kidd, L. Mandell, V. Pelosi, S. Ratti, V. Russo, L. Tallone, W. Zampieri, C. Caso, F. Coste, M. Dameri, G. Grosso, and G. Tomasini, Nuovo Cimento **49A**, 475 (1967).

[15] H. C. Dehne, J. Diaz, K. Stromer, A. Schmitt, W. P. Swanson, I. Borecka, G. Knies, and G. Wolf, Nuovo Cimento **53A**, 232 (1968).

[16] P. L. Connolly, W. E. Ellis, R. V. C. Hough, D. J. Miller, T. W. Morris, C. Ouannes, R. S. Panvini, and A. M. Thorndike, Brookhaven National Laboratory Report, 1967 (unpublished); Athens, Ohio Conference, 1967 (unpublished).

[17] E. W. Anderson, E. J. Bleser, G. B. Collins, T. Fujii, J. Menes, F. Turkot, R. A. Carrigan, Jr., R. M. Edelstein, N. C. Hien, T. J. McMahon, and I. Nadelhaft, Phys. Rev. Letters **16**, 855 (1966).

[18] I. M. Blair, A. E. Taylor, W. S. Chapman, P. I. P. Kalmus J. Litt, M. C. Miller, D. B. Scott, H. J. Sherman, A. Astbury, and T. G. Walker, Phys. Rev. Letters **17**, 789 (1966).